The implications of an idealised large-scale circulation for mechanical work done by tropical convection

The implications of an idealised large-scale circulation for mechanical work done by tropical convection

Jan A. Kamieniecki*, Maarten H. P. Ambaum and Robert S. Plant

Department of Meteorology, University of Reading, United Kingdom

Steven J. Woolnough

Climate, National Centre for Atmospheric Science, Department of Meteorology, University of Reading, Reading, United Kingdom

Corresponding author address: Department of Meteorology, University of Reading, Earley Gate, PO Box 243, Reading, RG6 6BB, UK

E-mail: j.a.kamieniecki@pgr.reading.ac.uk

ABSTRACT

A thermodynamic analysis is presented of an overturning circulation simulated by two cloud resolving models, coupled by a weak temperature gradient parametrisation. Taken together, they represent two separated regions over different sea surface temperatures, and the coupling represents an idealised large-scale circulation such as the Walker circulation. It is demonstrated that a thermodynamic budget linking net heat input to the generation of mechanical energy can be partitioned into contributions from the large-scale interaction between the two regions, as represented by the weak temperature gradient approximation, and from convective motions in the active warm region and the suppressed cool region. Model results imply that such thermodynamic diagnostics for the aggregate system are barely affected by the strength of the coupling, even its introduction, or by the SST contrast between the regions. This indicates that the weak temperature gradient parametrisation does not introduce anomalous thermodynamic behaviour. We find that the vertical kinetic energy associated with the large-scale circulation is more than three orders of magnitude smaller than the typical vertical kinetic energy in each region. However, even with very weak coupling circulations, the contrast between the thermodynamic budget terms for the suppressed and active regions is strong and is relatively insensitive to the degree of the coupling. Additionally, scaling arguments are developed for the relative values of the terms in the mechanical energy budget.

1. Introduction

The representation of the interactions between large-scale tropical circulations and local convective processes is an issue of fundamental importance to the simulation of tropical circulations. Computational constraints mean that models that explicitly simulate both convection and large-scale motion over domains of appropriate size can rarely be used. Hence a strategy, often adopted in the development of convection parametrisations for the tropics for GCMs, is to carry out studies using cloud resolving models (CRMs) that explicitly model convection in conjunction with a parametrisation of the large-scale dynamics that is influenced by local conditions. The weak temperature gradient approximation (Sobel and Bretherton 2000; Raymond and Zeng 2005) is one such parametrisation.

The atmospheric circulation can be analysed from the perspective of a generalized Carnot heat engine, that converts a temperature difference between two reservoirs into mechanical energy (e.g. Emanuel (1986) for the case of tropical cyclones). It has been shown by Pauluis (2011) that the impact of the hydrological cycle is to reduce the efficiency of such a conversion relative to the generalized Carnot maximum. This paper addresses convective and large-scale circulations as heat engines, unpacking how efficient they are at transforming potential work into kinetic energy dissipation and water lifting, in the face of the thermodynamic penalties associated with irreversible phase transitions in a moist atmosphere. Hitherto, similar analyses have not been applied in a context where the influence of large-scale circulations on local convection is modeled separately. Such an approach has the potential not only to clarify the consequences of different large-scale parametrisation approaches and to identify constraints on them but also to shed light on the nature of the interaction between the large-scale and the local dynamics. In particular, we

examine whether the mechanical energy budget is well-behaved when two convecting regions are coupled by a parametrised large-scale circulation.

The Weak Temperature Gradient (WTG) approximation was first suggested by Sobel and Bretherton (2000) and subsequently modified by introducing a short relaxation time (e.g. Raymond and Zeng 2005). Alternative methods such as the damped gravity wave (DGW) approach (Kuang 2008; Romps 2012), a spectral variant of the WTG (Herman and Raymond 2014) and others have been proposed. In this paper we focus on the weak temperature gradient approximation, but work on the DGW approach is ongoing. Preliminary analysis suggests that the DGW approach would give similar results to those presented in this paper.

A recent project has compared the results produced by different implementations of some of these methods (Daleu et al. 2015b, 2016), suggesting that the WTG approach is more prone to multiple equilibria than the DGW approach, and that the latter produces smoother large-scale vertical velocities. One of the advantages of the WTG approach is that its simplicity permits an analytical approach, and for that reason it is used here.

A common formulation of the WTG approximation assumes that a large-scale vertical wind is prescribed so as to contribute to the elimination of horizontal temperature contrasts. This paper adopts a typical definition, where the prescribed vertical large-scale wind w_{LS} is:

$$w_{LS}\frac{\partial \theta_r}{\partial z} = \frac{\theta'}{\tau} \quad , \tag{1}$$

where θ_r represents a reference profile for potential temperature, θ' a local potential temperature anomaly, τ a relaxation timescale, and z the height above sea level. w_{LS} is usually interpolated

to zero at the surface from the predicted value at the top of the planetary boundary layer and a minimum value for the static stability imposed. The time scale, τ , represents the strength of the coupling between regions and typical values of 2-3 hours can be justified as the spatial scale of the system being modeled ($\sim$500 km) divided by the speed of the fastest internal gravity waves ($\sim$50 m/s).

This circulation can be superimposed on the normal convective motions representing an idealised large-scale circulation that provides a linkage between two regions. Most studies have used a reference column approach, whereby the large-scale circulation is determined by temperature differences between the area modeled and an assumed environmental profile; more recently Daleu et al. (2012, 2015a) extended this approach to two coupled regions, which enables a more explicit representation of the consequences of the large-scale coupling mechanism. The reference column approach implies an infinite reservoir of energy and entropy, whereas by using coupled regions it is possible to analyse the mechanical energy budget of a closed system, separately attributing the contribution of the large-scale circulation described above and of the residual convective motions in the two regions.

The approach to the diagnosis of the mechanical work done by convection adopted in this paper broadly follows the isentropic perspective introduced by Pauluis and Mrowiec (2013) and Pauluis (2016). The conditional average of the vertical mass flux of air parcels, $\langle \rho w \rangle$, where ρ is the density of dry air and w is vertical velocity, is calculated in (z, θ_e) space, θ_e being the equivalent potential temperature. This is illustrated in Figure A1a. This conditionally averaged vertical mass

flux can be used to derive a streamfunction Ψ (Figure A1b):

$$\Psi(z,\theta_e) = \int_0^{\theta_e} \langle \rho w \rangle (z,\theta_e') \mathrm{d}\theta_e' \quad . \tag{2}$$

This describes mass flows in (z,θ_e) space and can be regarded as a a projection onto thermodynamic variables of the overturning circulation. It may be treated as a streamfunction providing divergent flows in that space do not exist. Likewise, conditional averages in (z,θ_e) space of variables such as temperature (T), vapour mixing ratio (r_v), liquid water mixing ratio (r_l), ice mixing ratio (r_i), entropy (S) and buoyancy (B) can be obtained. See Pauluis and Mrowiec (2013) for a further discussion of the merits of this approach.

Pauluis (2016) derives an approximate expression which relates components of work produced by a closed contour of the streamfunction which can be expressed as:

$$\underbrace{\oint T\mathrm{d}S}_{W_{T\mathrm{d}S}} - \underbrace{\sum_{w=v,l,i} \oint (-\mathscr{G}_w)\mathrm{d}r_w}_{\Delta\mathscr{G}} \approx \underbrace{\oint B\mathrm{d}z}_{W_b} + \underbrace{g\oint r_T \mathrm{d}z}_{W_p} \quad , \tag{3}$$

where $r_T = r_v + r_l + r_i$ is the total water mixing ratio, g represents the acceleration due to gravity and $\mathscr{G}_w$ the specific Gibbs free energy for the various phases of water represented in the model. $W_{T\mathrm{d}S}$, the first item on the left hand side of this equation, can be interpreted as the work that would be done by a generalized Carnot engine with the same path in (T,S) coordinates. The second term, $\Delta\mathscr{G}$, referred to as the "Gibbs penalty", is the lost part of that work that is needed to evaporate liquid water at below saturation into the system in order to maintain the mean humidity profile against the hydrological cycle and is discussed in detail in Pauluis and Held (2002a,b) and Pauluis (2011). The first term on the right hand side, W_b, is the generation of kinetic energy by resolved motions in the model and the second, W_p, the increase in geopotential energy of the water content lifted by convection. Ultimately, the buoyancy term W_b generates kinetic motion

of air which is dissipated through turbulent processes mostly near the surface and the moisture elevator term W_p generates potential energy in hydrometeors which is subsequently dissipated through friction during precipitation (Pauluis et al. 2000). The Gibbs penalty term does not correspond to external energy transiting through the system, but serves to limit the work available for conversion into mechanical energy. In this sense, the Gibbs penalty is the part of the entropy budget that needs to be expended to maintain the composition changes in the hydrological cycle, and that therefore cannot be used to produce mechanical work.

The terms in this equation can be represented by thermodynamic diagrams of streamfunction contours in the appropriate spaces, for example that for $W_{T\mathrm{d}S}$ in (S,T) space. A weighted total of integrals along equally spaced contours of Ψ is used to calculate values of the terms in Eq. 3 for the entire system. Figure A2 shows contours for the most significant terms in the case of a single region in radiative-convective equilibrium for the model configuration described below.

This paper applies the diagnostic approach outlined above to unpack the generation of mechanical work by a modeled overturning circulation superimposed on convective processes. In particular it analyses the relationship between the strength of WTG coupling and the strength of the circulation, partitioned into contributions from the large-scale circulation and convective circulations in relatively cool/dry and warm/moist regions, in order to deepen understanding of how the large-scale circulation can suppress or enhance convection. The impact of varying the SST difference between the regions is also analysed.

The paper is organised as follows. Section 2 explains how an isentropic analysis can be applied to two coupled regions and also suggests a refinement that improves the accuracy of the decom-

position for an anelastic model. Section 3 briefly describes the CRM used and presents numerical results for the mechanical energy budget, partitioned into a large-scale circulation and convective localised flows for varying strengths of coupling as well as further results for varying SST differences between the two regions. Section 4 develops an analytical expression for the generation of kinetic energy by the WTG coupling, which is seen to be consistent with results obtained from the CRM. Scaling arguments are also developed for comparison with other results obtained by the CRM. The implications of this study are discussed and some conclusions are drawn in Section 5.

2. Isentropic diagnostic framework

a. General approach

As in Pauluis (2016), entropy is expressed as specific entropy per unit mass of dry air:

$$s = s_d + r_v s_v + r_l s_l + r_i s_i \quad , \tag{4}$$

where s_d is the specific entropy of dry air, and s_w for $w = v, l, i$ are the specific entropies of the three phases of water. In order to achieve a one-to-one relationship between equivalent potential temperature and this specific entropy, the former is defined as:

$$\theta_e = T_0 \ln \frac{s}{c_p} \quad , \tag{5}$$

where T_0 is the temperature at the triple point of water and c_p is the heat capacity of dry air at constant pressure.

Pauluis (2016) uses a weighted average of equally spaced contours of the streamfunction over the region where $\Psi < 0$ to calculate the components of overall work throughput of the system as expressed in Eq. 3. Following that approach, these integrals are calculated here along contours of the streamfunction in (z, θ_e) space, using the conditionally averaged values of the variables required for the calculation (such as T, S for $W_{T\mathrm{d}S}$ etc.) of the points defining the trajectory, rather

than seeking first to determine a streamfunction in (T,S) space and then to calculate contour integrals in that space. The same results can also be calculated using appropriate surface integrals of the streamfunction, e.g. the first term on the left hand side of Eq. 3 becomes $\iint \Psi \mathrm{d}S\mathrm{d}T$ over the same domain. Although the results shown in this paper are calculated using contours, the surface integral approach is important in justifying the partitioning approach described below.

b. Extension to two region case

This paper applies the decomposition of work done discussed above to a two-region system, where the regions are coupled by a large-scale circulation consisting of vertical winds specified by the WTG approximation. The cooler region is identified by a subscript 1 and represents a fraction $1-\varepsilon$ of the total area, and the warmer region (subscript 2) a fraction ε (all the numerical results shown in this paper are based on $\varepsilon = 0.5$). When a temperature difference between the surfaces underlying the two regions gives rise to a large-scale circulation, there will be mass transfers between the two regions and the contours of the integral of the vertical mass flux (as in Eq. 2) in each region will not be closed, making it impossible to estimate the components of Eq. 3 within each region using either contour or surface integrals (the latter requiring a domain bounded by a constant value of the streamfunction).

One could, of course, merge the two regions prior to performing any analysis, but this introduces significant error as the dynamics are generally influenced by local rather than merged values of fields (e.g. buoyancy for $W_b = \oint B\mathrm{d}z$), and such a method will not permit a partitioning of the components of work done to localised features in each region and to the large scale circulation.

Instead, one can identify and separate out the vertical large-scale velocities $w_{LS,1}(z), w_{LS,2}(z)$ (obtained from the values of $\Psi(z,\theta_e)$ as $\theta_e \to \infty$ and the dry air mass distribution in each region). The circulations calculated using Eq. 2 for convective local velocities $w_i^* = w_i - w_{LS,i}$ $(i = 1,2)$ in each region will now be closed, as will that in a notional third "region" which consists of the total of the large-scale circulation within the two regions, weighted by their relative areas, since $(1-\varepsilon)w_{LS,1} + \varepsilon w_{LS,2} = 0$. These streamfunctions are additive by construction:

$$\Psi_1 + \Psi_2 = \Psi_1^* + \Psi_2^* + \Psi_{LS} \quad , \tag{6}$$

where $\Psi_{1,2}$ are the observed circulations in each region, $\Psi_{1,2}^*$ represent the adjusted local circulations and Ψ_{LS} is the large-scale circulation. The respective surface integrals will also be additive, providing that a domain is selected that is bounded by a contour for which all the $\Psi = 0$ and that $\Psi \leqslant 0$ throughout that domain (which should generally be possible for a sufficiently smooth system). This additivity is important because it means that the partitioning of work in Eq. 3 can also be extended to the components of the coupled two-region system. For example:

$$W_{T\mathrm{d}S} = \iint \Psi_1^* \mathrm{d}S\mathrm{d}T + \iint \Psi_2^* \mathrm{d}S\mathrm{d}T + \iint \Psi_{LS} \mathrm{d}S\mathrm{d}T \tag{7}$$

Since the surface integrals are additive, a calculation of these quantities using contour integrals will also be additive. An example of this partitioning can be seen in Figure A3.

As has been mentioned, these integrals are calculated for the entire system using weighted trajectories along contours of the streamfunction in (θ_e, z) space, and with averaged values for the other quantities required for the calculation. The values are calculated separately for each region while for the large-scale circulation a mean value is taken, weighted by the contribution of each region to that point in the combined thermodynamic space. As a result of this, the calculation of the large-scale terms is more approximate.

c. Anelastic case

The derivation of Eq. 3 uses the hydrostatic approximation for the reference profile, where the total pressure of all gases in the atmosphere (i.e. dry air and water vapour) is related to height. In the case of an anelastic model, such as the Met Office's Large Eddy Model (LEM) which is used to derive the numerical results in this paper, it is the partial pressure of dry air that is assumed to be in hydrostatic equilibrium in the reference profile, and as will be seen the balance of Eq. 3 can be improved by a small correction which is conveniently included in the water vapour component of the Gibbs penalty term and is derived in Appendix A.

3. Model description and results

a. Model setup

The numerical simulations in this section have been produced using a configuration of version 2.4 of the Met Office's Large Eddy Model (LEM) in cloud-resolving mode amended to investigate the effect of coupling two regions via the WTG in an idealised context. The underlying LEM is described in Gray et al. (2001) and more complete details of the configuration used here can be found in Daleu et al. (2012). The microphysics are represented by a five-category prognostic scheme, with mixing ratios for cloud water, rain, ice, graupel and snow and with number concentrations for ice, graupel and snow. Each region is modelled in a two-dimensional configuration with a width of 128km (resolution of 500m) and a height of 20km (60 vertical levels). A fixed tropospheric cooling profile is used rather than interactive radiation; In order to isolate the effect of the coupling strength, a fixed tropospheric cooling profile is used rather than interactive radiation. The cooling rate is fixed at 1.5 K/day below 220 hPa, and decreases linearly with pressure to 0 K/day at 120 hPa, corresponding to integrated atmospheric cooling

close to 150Wm^{-2}, depending on the precise value of the surface pressure .The sub-grid model is parametrised using a modified first order Smagorinsky-Lilly approach. For consistency with previous studies with this model a mixing length of 250m was used, but the impact of this choice on the conclusions of this paper was tested and found to be minor.

The WTG velocity is specified by the region-mean potential temperature difference between the two regions and is used to perform advection of both temperature and moisture between the two regions. The two regions are of equal size and the temperature difference at the surface between them, ΔT_s, unless otherwise specified, is set to 2K (302.7K and 304.7K for each region). The LEM is run to equilibrium for a 120 day duration (although no diurnal cycle is modeled), with the first 20 days discarded from the analysis to avoid any transient features, and results are obtained every 30 minutes, giving 4,800 samples of the required variables.

The LEM includes a considerable number of approximations, particularly with respect to the thermodynamics of the system. For example, the specific heat capacities of liquid water and water vapour are taken to be equal (and effectively zero) and the specific enthalpy of water vapour L_v does not depend on temperature; these are not consistent with the more exact approach underlying Eq. 3 that is implemented in the diagnostics. Although these approximations are not ideal, the application of a more sophisticated diagnostic framework to motions and variable values derived from a simplified model still provides insight into the full thermodynamic processes that are approximated in the LEM. This choice of model configuration involves a number of compromises that facilitate multiple long simulations over a more detailed representation of the features being modelled, consistent with the idealised nature of the experiments described.

b. Results for single region

The model was first run for an uncoupled single region over 302.7K sea-surface temperature. The resulting thermodynamic diagrams (Figure A2) have already been mentioned. Values for the work terms can be seen in Table A1, in which the effect of the modification described in Appendix 1 is also identified. For comparison, the reference case values calculated in Pauluis (2016, Table 1) are also shown.

It will be seen that the values obtained here are in general some 30% higher than those in Pauluis (2016). Comparison of the W_p thermodynamic diagrams (Figure A2b in this paper and 4c in Pauluis (2016)) indicates that the atmosphere modeled here has a significantly higher total water mixing ratio, partially explained by the choice of model parameters to represent conditions in the Western Pacific – for example the SST for these simulations is 2.2K higher than in Pauluis (2016). Likewise, the $W_{T\mathrm{d}S}$ diagram (Figure A2d in this paper and 4a in Pauluis (2016)) shows higher values for entropy, and slightly higher temperatures. The relative values of the mechanical work components are consistent between the two models, and consistent with scaling arguments which are developed below.

c. Dependency of components of work done on strength of coupling

In order to investigate the impact of the coupling on the generation of mechanical work in the two regions, simulations were performed with values of the WTG timescale τ between 1 hour and 50 hours; results for two uncoupled regions are also shown for comparison ($\tau = \infty$). It will be seen that values of the components of work done for the total system remain broadly constant (Figure A4a), although the introduction of coupling produces a marginal increase in W_b and $W_{T\mathrm{d}S}$

which then decreases as the coupling increases.

Values for the local circulations in each of the regions (Figures A4c and A4d) on the other hand exhibit a significant difference from the overall mean. This difference is already marked at very weak coupling and increases as the value of τ decreases, although the values for the cooler region remain almost constant for $\tau < 10$ hrs, possibly reflecting the fact that the region approaches a humidity minimum (Figure A5). Column integrated water vapour in that region decreases significantly between τ = 50 hours and τ = 10 hours and then shows less variation, indeed a slight increase for $\tau < 5$ hours. As the cooler region dries, the relative importance of the Gibbs penalty component will increase. Weaker convection is associated with a disproportionate decrease in the buoyancy component, as discussed in Pauluis (2016). Figure A6 shows the vertical mass flux for the two regions for $\tau = 50$ hrs which confirms that convection in the cooler region is markedly suppressed even for such weak coupling.

The large-scale circulation (Figure A4b) shows a different pattern; this includes both regions, which maintain a temperature difference, and hence W_b plays a more prominent role, reducing as the coupling increases and the temperature difference decreases. This decrease is partly compensated by a slight increase in W_p as a stronger circulation lifts more moisture. The Gibbs penalty increases with the coupling up to a maximum at around τ = 5 –10 hrs before decreasing; this can be attributed to increasing coupling first leading to drying of the cooler region and hence to a decrease in the relative humidity at which energy enters the system (see the scaling arguments below for how this impacts $\Delta\mathscr{G}$ non-linearly). As discussed above, as τ decreases below 5 hours the cooler region marginally moistens which contributes to the increase in $\Delta\mathscr{G}$. The mechanical work terms for components of the large-scale circulation for strong coupling

297 are similar in magnitude to those for the localised circulation in the cooler region; both are
298 substantially smaller than those for the warmer region. As previously mentioned, the balance in
299 the large-scale circulation is more approximate than for the other components, and in fact is not
300 improved by inclusion of the correction term described in Appendix A.
301

302 *d. Components of kinetic energy*

303 The relationship between the strength of the coupling and components of kinetic energy in the
304 total system is shown in Figure A7. The coupling has an insignificant effect on the kinetic energy
305 in the aggregate system, but a strong influence on the vertical kinetic energy associated with the
306 large-scale circulation, which increases with coupling strength. The increase in vertical kinetic
307 energy for smaller τ indicates that the effect of reducing τ in increasing w in Eq. 1 is stronger
308 than the effect that enhanced coupling has on reducing the temperature contrast θ' between the
309 regions.
310

311 A similar comparison between large-scale and convective horizontal components of kinetic
312 energy would require further assumptions as to the distance between the two regions and their
313 geometry. From a thermodynamic perspective, horizontal motion is of less relevance to the
314 generation of mechanical energy, as it traverses only a small temperature contrast (as forced by the
315 coupling). It is true to say that the horizontal near-surface flow will likely contribute substantially
316 to the total frictional dissipation in the real system, but in our modelled system this dissipation is
317 constrained to occur in the two regions.
318

This comparison between large-scale and convective vertical kinetic energies indicates how weak the large-scale circulation is when compared with convective motions. Despite this, the introduction of a large-scale circulation through WTG coupling has very noticeable effects on the strength and nature of the convection within the two regions. In the absence of this large-scale circulation the mechanical energy budgets in the two regions are very similar. However, even with a very weak large-scale overturning circulation, convection in the warm region is markedly enhanced and that in the cool region suppressed.

e. Dependence on SST difference between the regions

A further set of numerical experiments was performed for strong coupling (τ = 2 hours) where the temperature difference between the two regions was varied between 0K and 2K. In each experiment, the regions were of equal area and the mean SST of the aggregate system was 303.7K. Plots of the components of the mechanical budget are shown in Figure A9. As in the experiment with varying coupling strength, the values of the four components of the mechanical work budget remain broadly constant for the system in aggregate, independent of the SST difference. The values for the cool and warm regions coincide for ΔT_s=0 and then diverge gradually. The components of the budget for the large-scale circulation exhibit a quadratic dependency on ΔT_s redfor low values of ΔT_s (see also the log plot in Figure A10) which is discussed below.

4. Analytical expressions and scaling

a. Energy conversion under the Weak Temperature Gradient Approximation

The simple form of the WTG means that it is possible to derive an analytical expression for the rate of conversion of potential energy into kinetic energy that it implies. Following Romps (2012) one can express the thermodynamic equation for a one-dimensional WTG system in height

coordinates as follows:

$$\frac{\partial B}{\partial t} = -N^2 w + Q \quad , \tag{8}$$

where $B = \frac{g\theta'}{\theta}$ is the dry buoyancy , N is the local Brunt-Väisälä frequency ($N^2 = -\frac{g}{\theta}\frac{\partial \theta}{\partial z}$), and Q is the external heat input into the system. It is assumed that N does not have any dependency on time although it can vary with height.

If the WTG approximation is used, the vertical velocity (above the boundary layer) can be expressed as:

$$w = \frac{\theta'}{\tau \frac{\partial \theta}{\partial z}} = \frac{B}{\tau N^2} \quad . \tag{9}$$

The Available Potential Energy (APE) introduced by Lorenz (1960), $\bar{A}$, of the system can be described locally in terms of these variables by dry "availability" $A = \frac{B^2}{2N^2}$. It can be shown that the density-weighted column integral of A is equal to $\bar{A}$. The time derivative of the local availability is given by:

$$\frac{\partial A}{\partial t} = \frac{2B}{2N^2}\frac{\partial B}{\partial t} = \frac{BQ}{N^2} - Bw = \frac{BQ}{N^2} - \frac{2A}{\tau} \quad . \tag{10}$$

This can be interpreted as indicating that availability is increased by a differential heating term $\frac{BQ}{N^2}$ which is balanced by a conversion term from potential to kinetic energy of:

$$C_{A\rightarrow KE} = \frac{2A}{\tau} \quad . \tag{11}$$

Thus for the system as a whole (ignoring the complication of the boundary layer interpolation) the conversion to kinetic energy will be $\frac{2\bar{A}}{\tau}$. It will also be noted that Eq. 10 requires heat input to correlate with positive buoyancy, which is consistent with the second law of thermodynamics. The effect of the boundary layer interpolation is to weaken the coupling in the lowest layers, which can

be represented by increasing the value of τ for those layers - the impact of this adjustment is minor.

Figure A8 compares the conversion term from Eq. 11 and the large-scale components of the mechanical energy budget as in Figure A4b, which of course includes moist variables. The mechanical work done terms W_b scales as $\frac{2\bar{A}}{\tau}$, in fact the values coincide. As the APE has a quadratic dependency on the temperature difference between the two regions (which will in turn depend linearly on the temperature difference at the surface), a quadratic dependency of the work terms on ΔT_s may be anticipated. This is indeed seen in Figure A9b as presented in Section 3e - a log-log plot of the same values is shown in Figure A10.

b. Scaling for components of work done

Further scalings can be developed for the relative values of the terms in the mechanical energy budget. These do not depend on the assumption of a coupling mechanism. In an anelastic model such as the LEM, the buoyancy (see Gray et al. (2004, Eq. 11 - 13)) is calculated as:

$$B = g\left(\frac{\theta'}{\theta_r} + \left(\frac{R_v}{R_d} - 1\right) r_v - \sum_{w \neq v} r_w\right) \quad , \tag{12}$$

where R_v and R_d are the specific gas constants for water vapour and dry air and θ_r is the reference-state potential temperature. Hence, if we assume that variations in specific humidity dominate the buoyancy rather than any temperature differences as is suggested by these model results, and also that $\delta r_T \approx \delta r_v$, only the second term in Eq 12 need be considered for scaling purposes. Hence the buoyancy lifting term, W_b in Eq. 3 , will scale as $(\frac{R_v}{R_d} - 1)W_p = 0.6 \times W_p$, with W_p being the moisture lifting term. The approximate scaling between W_b and W_p can be readily verified from the numerical values shown in Table A1 and also holds for the warmer region for the two-region system (Figure A4d) which dominates the aggregate system (Figure

A4a). In circumstances where the temperature differences are significant (and correlated with moisture anomalies), such as for the large-scale circulation at low coupling strength one could expect $\frac{W_b}{W_p}$ to have a value greater than 0.6 as is observed (Figure A4b).

Pauluis (2011, Eq. 25) gives an expression for the Gibbs penalty. Assuming that condensation occurs close to saturation, that vapour anomalies dominate as before and that the sensible heat component is negligible, an approximate expression for this term can be written in terms of the net rate of evaporation at the surface $E = \frac{\Delta r_v}{\Delta t}$:

$$\Delta\mathscr{G} \approx -R_v T_{\text{out}} E \ln \mathscr{H}_{\text{in}} \tag{13}$$

where $\mathscr{H}$ is relative humidity and the subscripts $_{\text{in}}$, $_{\text{out}}$ indicate conditional harmonic means over the zones where heat enters and leaves the system. For example, if we write F_{in} for heat input and $\mathscr{A}$ as the system's boundary then following Ambaum (2010, Eq. 10.50):

$$\frac{1}{T_{\text{in}}} = \left(\int_{\mathscr{A}} F_{\text{in}} \, d\mathscr{A} \right)^{-1} \int_{\mathscr{A}} \frac{F_{\text{in}}}{T} d\mathscr{A} \, . \tag{14}$$

T_{out} is defined likewise using F_{out}, the heat output of the system, and $\mathscr{H}_{\text{in}}$ is defined as in Pauluis (2011, Eq. 16).

Likewise, W_{TdS} will be mainly driven by the latent heat input and scales with the generalized Carnot efficiency:

$$W_{TdS} \approx \frac{T_{\text{in}} - T_{\text{out}}}{T_{\text{in}}} \left(L_v E + \Delta\mathscr{G} \right) \tag{15}$$

$$\approx \frac{T_{\text{in}} - T_{\text{out}}}{T_{\text{in}}} L_v E \quad , \tag{16}$$

where L_v is the enthalpy of vaporisation of water. It will be seen from Eq. 13 that the Gibbs penalty term can be neglected in scaling Eq. 15, given that $\frac{R_v T_{\text{out}}}{L_v} \approx 0.05$. Eliminating E between Eqs 13 and 16:

$$\Delta\mathscr{G} \approx -\frac{R_v T_{\rm out} T_{\rm in}}{L_v (T_{\rm in} - T_{\rm out})} \ln \mathscr{H}_{\rm in} W_{TdS} \quad . \tag{17}$$

Values of 295 K for $T_{\rm in}$ and 280 K for $T_{\rm out}$ can be obtained from the model (or even by inspection of Figure A2d which shows values for the RCE case, which will also be typical for the aggregate system). An average value for $\mathscr{H}_{\rm in}$ is more problematic to define, but using 60% is consistent with model results and the observed values of $\Delta\mathscr{G} \approx 0.5 W_{TdS}$.

It is possible to develop Equation 17 further by making use of the Clausius-Clapeyron relation in the form $\frac{{\rm d}e_s}{e_s} = \frac{L_v {\rm d}T}{R_v T^2}$:

$$\frac{\Delta\mathscr{G}}{W_{TdS}} \approx -\frac{R_v T_{\rm out} T_{\rm in}}{L_v (T_{\rm in} - T_{\rm out})} \ln \mathscr{H}_{\rm in} \quad , \tag{18}$$

$$\approx \frac{\ln \mathscr{H}_{\rm in}}{\ln \frac{e_{s,\rm out}}{e_{s,\rm in}}} \quad , \tag{19}$$

where $e_{s,\rm in}$ and $e_{s,\rm out}$ are the saturated vapour pressures of water at temperatures $T_{\rm in}$ and $T_{\rm out}$. Defining $r_{v,\rm in}$ as the vapour mixing ratio corresponding to $\mathscr{H}_{\rm in}$ at temperature $T_{\rm in}$ and dry pressure $p_{d,\rm in}$:

$$\frac{\Delta\mathscr{G}}{W_{TdS}} = \frac{\ln \frac{R_v r_{v,\rm in} p_{d,\rm in}}{R_d e_{s,\rm out}} + \ln \frac{e_{s,\rm out}}{e_{s,\rm in}}}{\ln \frac{e_{s,\rm out}}{e_{s,\rm in}}} \quad , \tag{20}$$

We now introduce $r_{vs,\rm out}$ via $e_{s,\rm out} = R_v / R_d p_{d,\rm out} r_{vs,\rm out}$ where $p_{d,\rm out}$ is the partial pressure of dry air at temperature $T_{\rm out}$. Substituting for $e_{s,\rm out}$ in the first logarithm in the numerator of Eq. 20 leads to:

$$\frac{\Delta\mathscr{G}}{W_{TdS}} = 1 - \frac{\ln p_{d,\rm out}/p_{d,\rm in}}{\ln e_{s,\rm out}/e_{s,\rm in}} - \frac{\ln r_{vs,\rm out}/r_{v,\rm in}}{\ln e_{s,\rm out}/e_{s,\rm in}} \quad . \tag{21}$$

Assuming that $r_{vs,\mathrm{out}} \lesssim r_{v,\mathrm{in}}$ (see Figure A2b to confirm that this is reasonable for all but the shallowest circulations):

$$\frac{\Delta \mathscr{G}}{W_{TdS}} \lesssim 1 - \frac{\ln \frac{p_{d,\mathrm{out}}}{p_{d,\mathrm{in}}}}{\ln \frac{e_{s,\mathrm{out}}}{e_{s,\mathrm{in}}}} \tag{22}$$

$$\tag{23}$$

Making a Taylor expansion in $\ln(1+x) \approx x$:

$$\frac{\Delta \mathscr{G}}{W_{TdS}} \lesssim 1 - \frac{\frac{\Delta z}{H^*_{pd}}}{\frac{\Delta z}{H^*_{es}}} \tag{24}$$

$$\lesssim 1 - \frac{H^*_{es}}{H^*_{pd}} \tag{25}$$

$$\lesssim 1 - \frac{R_v g \bar{T}}{R_d L_v \Gamma} \quad , \tag{26}$$

where Δz is the height difference between the in and out states, and $H^*_{es} = \frac{-R_v \bar{T}^2}{L_v \Gamma}$, $H^*_{pd} = \frac{R_d \bar{T}}{g}$ are the scale heights for saturated vapour pressure and the partial pressure of dry air, $\bar{T}$ is an average temperature over the cycle between T_{in} and T_{out} and Γ is the atmospheric lapse rate. Using $\bar{T} = 290\mathrm{K}$ and $\Gamma = -5\mathrm{km}^{-1}$ gives $\frac{\Delta \mathscr{G}}{W_{TdS}} < 0.64$. This ratio will decrease as $\frac{r_{v,\mathrm{out}}}{r_{v,\mathrm{in}}}$ decreases, i.e. as the temperature difference between the "in" and "out" states increases.

Combining these various elements as in Eq. 3, one can expect the efficiency with which such a system in aggregate generates mechanical work W_b to be typically 20% of the generalized Carnot maximum W_{TdS}. The values shown in Table A1 and in Figure A4 are consistent with these scalings.

There is an imbalance in latent heat input between the regions, consistent with the transport of moisture from the cool region to the warm region. The Gibbs penalty component of the mechanical energy budget for the large-scale circulation is strongly correlated with this moisture transport between the regions (Fig. A11). The relationship between these two quantities can be explained

using Eq. 13, using the net moisture advected by the large-scale circulation:

$$\Delta\mathscr{G} \approx \frac{-R_v}{L_v} T_{\text{out}} \ln \mathscr{H}_{\text{in}} \times \text{latent heat transport} \quad . \tag{27}$$

Using $T_{\text{out}} = 285\text{K}$ and $\mathscr{H}_{\text{in}} = 60\%$ as before provides a good fit.

5. Summary and discussion

This paper shows how the mechanical energy budget for a convecting system proposed in Pauluis (2016) can be applied in the case of two coupled regions, permitting attribution of each of the components to either localised features within one of the two regions or to the large-scale circulation. It also proposes a refinement to the basic approach in the case of an anelastic cloud resolving model. Our work has not identified any energetic inconsistencies introduced by the use of the WTG approximation as a proxy for large-scale circulation.

Numerical results were obtained using a CRM in which two regions are coupled using the WTG approximation. They demonstrate that theterms in the mechanical energy budget of the system considered as a whole are insensitive to the strength (indeed even the presence) of the coupling, indicating that the coupling does not distort the energy balance of the whole system. However, even very weak coupling has a marked effect on the nature of the convection within each region and its associated energy budget terms. As the strength of the coupling increases the convection in the cool region is further suppressed and that in the warmer region enhanced. It is possible that some of this insensitivity is a consequence of using a fixed cooling profile rather than an interactive radiative model. However, other broad properties of the system appear to be independent of the coupling strength which suggests that an interactive radiative scheme would be likely to produce similar results. Further numerical experiments show that the mechanical energy

budget for the entire system is equally insensitive to changes in the difference in SSTs between the columns.

The ratios between the component terms contributing to the total energy flows for the entire system and for each of the regions (where the effect of the large-scale velocity is isolated) are relatively constant as a function of coupling strength and are consistent with estimates obtained by theoretical scaling arguments. On the other hand, the values of the component terms for the large-scale circulation exhibit markedly different features in that the buoyancy contribution is more significant than that due to the lifting of precipitation while the Gibbs penalty reaches a maximum as the cooler region dries out, before then decreasing as the differences between the regions are eliminated with stronger coupling.

The buoyancy contribution to the large-scale circulation is consistent with that predicted from an analytical approach to the energetics implied by WTG in a dry setup which also predicts its quadratic dependency on the SST difference between the columns that is observed. We also present more general scaling arguments for the components of a mechanical energy budget, which could serve to indicate the impact of changing atmospheric conditions on the generation of kinetic energy.

The vertical kinetic energy associated with the large-scale circulation is found to be more than three orders of magnitude smaller than the vertical kinetic energy associated with the convection within each region. Despite this weak magnitude, the coupling has a strong influence on the suppression and enhancement of convection in each of the regions. The imposition of the WTG approximation may be interpreted as a representation of the requirement for low temperature

gradients in the tropics due to weak rotational effects. In this sense, the contrast in local convective intensity can be seen as the consequence of a large-scale dynamical constraint and not as a local result of contrast in SSTs.

The techniques introduced in this paper, suitably modified, can be applied to reanalysis products to estimate a mechanical work budget for large-scale circulations such as the Walker or Hadley circulations, which would provide further insight into whether coupling techniques such as the WTG provide a useful approach to reflecting such phenomena in studies of convection. Similarly, they could shed light on the mechanics of convective aggregation, which can be studied using the WTG approximation (Emanuel et al. 2014).

Acknowledgments. Jan Kamieniecki is supported by a grant from the UK Natural Environment Research Council [grant number NE/K004034/1]. We would like to thank the Met Office for access to version 2.4 of the LEM, C L Daleu for making her model configuration available to us and David Raymond, Timothy W. Cronin and one anonymous reviewer for their helpful comments.

APPENDIX A

Components of work done in an anelastic model

In this appendix we explain how the derivation of the components of work (Eq. 3) in Pauluis (2016) can be refined in the case of an anelastic model and we derive an approximate expression for a suggested correction term.

a. Hydrostatic balance in an anelastic context

The original derivation of Eq. 3 involves the use of the hydrostatic approximation $\mathrm{d}p = -\rho_{\mathrm{ref}} g \mathrm{d}z$ in evaluating $-\alpha_d \mathrm{d}p$, where ρ_{ref} is the density of dry air in the reference profile and α_d is the

specific volume of dry air. In an anelastic model such as the LEM, this need not hold in general, but it does hold for the reference profile, where it relates the partial pressure of dry air p_0 to height: $\mathrm{d}p_0 = -\rho_{\mathrm{ref}} g \mathrm{d}z$.

b. Derivation of approximate correction term

The original derivation of Eq. 3 can be restated as below:

$$\oint T \mathrm{d}s = -\oint \alpha_d \mathrm{d}p - \sum_{w=v,l,i} \oint g_w \mathrm{d}r_w \quad , \tag{A1}$$

where:

$$\alpha_d = \frac{R_d T + r_v R_v T}{p} \tag{A2}$$

$$\approx \frac{R_d T_{\mathrm{ref}}}{p} \left(1 + \frac{T' + r_v (\frac{R_v}{R_d}) T_{\mathrm{ref}} - r_T T_{\mathrm{ref}}}{T_{\mathrm{ref}}} + r_T \right) \tag{A3}$$

$$= \frac{R_d T_{\mathrm{ref}}}{p} \left(1 + \frac{B}{g} + r_T \right) \quad , \tag{A4}$$

using the definition of B in Eq. 12, and where R_d and R_v are the specific gas constants for dry air and water vapour respectively, and T_{ref} the temperature of the reference profile, ignoring expressions that are second order in the mixing ratio or buoyancy. Likewise, one can then approximate the contour integrals of the second and third terms on the right hand side of Eq. A4:

$$-\oint \frac{R_d T_{\mathrm{ref}} B}{g p} \mathrm{d}p \approx -\oint \frac{R_d T_{\mathrm{ref}} B}{g p_0} \mathrm{d}p_0 = \oint B \mathrm{d}z \tag{A5}$$

$$-\oint \frac{R_d T_{ref} r_T}{p} \mathrm{d}p \approx \oint g r_T \mathrm{d}z \quad . \tag{A6}$$

The contour integral of the first term on the right hand side of A4 is zero for an anelastic model if the full hydrostatic approximation is used as in Pauluis (2016). Applying instead the hydrostatic approximation for dry air, it can be simplified with the assumption that the reference profile is

close to the equilibrium state and that variations in the pressure of dry air at a given height are insignificant when compared with variations in water vapour pressure, (ie $p \approx p_{\rm ref} + e$) and ignoring higher orders of $\frac{e}{p_{\rm ref}}$ to obtain an additional term:

$$-\oint \frac{R_d T_{\rm ref}}{p} \mathrm{d}p = -\oint \frac{R_d T_{\rm ref}}{p_{\rm ref}+e} \mathrm{d}(p_{\rm ref}+e) \tag{A7}$$

$$\approx -\oint \frac{R_d T_{\rm ref}}{p_{\rm ref}} \mathrm{d}p_{\rm ref} + \oint \frac{e R_d T_{\rm ref}}{{p_{\rm ref}}^2} \mathrm{d}p_{\rm ref} - \oint \frac{R_d T_{\rm ref}}{p_{\rm ref}} \mathrm{d}e \quad . \tag{A8}$$

Making use of the gas law:

$$-\oint \frac{R_d T_{\rm ref}}{p} \mathrm{d}p \approx -\oint \frac{1}{\rho_{\rm ref}} \mathrm{d}p_{\rm ref} + \oint \frac{e R_d T_{\rm ref}}{p_{\rm ref}^2} \mathrm{d}p_{\rm ref} - \oint \frac{R_d T_{\rm ref}}{p_{\rm ref}} \mathrm{d}e \quad . \tag{A9}$$

Using the hydrostatic approximation, and remembering that $e = r_v \frac{R_v}{R_d} p_{\rm ref}$:

$$-\oint \frac{R_d T_{\rm ref}}{p} \mathrm{d}p \approx \oint g \mathrm{d}z + \oint \frac{r_v R_v T_{\rm ref}}{p_{\rm ref}} \mathrm{d}p_{\rm ref} - \oint \frac{r_v R_v T_{\rm ref}}{p_{\rm ref}} \mathrm{d}p_{\rm ref} - \oint R_v T_{\rm ref} \frac{\mathrm{d}r_v}{d p_{\rm ref}} \mathrm{d}p_{\rm ref} \quad . \tag{A10}$$

The first of the terms on the right hand side is zero, and the second and third cancel, leaving the final term, which can be expressed as an integral in r_v:

$$-\oint \frac{R_d T_{\rm ref}}{p} \mathrm{d}p \approx -\oint R_v T_{\rm ref} \mathrm{d}r_v \quad . \tag{A11}$$

This expression can be integrated by parts and then expressed in terms of an integral in z:

$$-\oint \frac{R_d T_{\rm ref}}{p} \mathrm{d}p \approx +\oint R_v r_v \mathrm{d}T_{\rm ref} = -\oint R_v r_v \Gamma \mathrm{d}z \quad , \tag{A12}$$

where Γ is the lapse rate of the reference profile. Eq. A11 is the form of the equation that is used to calculate this term numerically in the contour integrals, Eq. A12 provides a more useful form in developing scaling arguments below.

The new term in the form shown in Eq. A11 bears a similarity to a term in the water vapour component of the Gibbs penalty $\oint (-\mathscr{G}_v) \mathrm{d}r_v$, depending as it does on the same state variables since:

$$\mathscr{G}_v = c_l \left(T - T_f - T \ln \frac{T}{T_f} \right) + R_v T \ln \mathscr{H} \tag{A13}$$

where c_l is the specific heat capacity of liquid water at constant pressure, T_f its freezing temperature and $\mathscr{H}$ the relative humidity. One can therefore introduce a modified specific Gibbs free energy for the vapour state:

$$\mathscr{G}^*{}_v = c_l \left(T - T_f - T \ln \frac{T}{T_f} \right) + R_v T (1 + \ln \mathscr{H}) \tag{A14}$$

and (neglecting a term in $T_{\mathrm{ref}} - T$) instead of Eq. 3 one can write:

$$\oint T \mathrm{d}S \approx \oint B \mathrm{d}z + \oint r_T g \mathrm{d}z + \sum_{w=v,l,i} \oint (-\mathscr{G}^*_w) \mathrm{d}r_w \tag{A15}$$

where $\mathscr{G}^*_w = \mathscr{G}_w$ for $w = l, i$. (It could be argued that from a physical perspective this term is a correction to the mechanical work generated and should therefore instead be combined with W_b.)

c. Numerical values and scalings

The contribution of this new term can be illustrated by comparing numerical values for the components of Eq A15 with the modified version produced by the LEM for the case of a single uncoupled convecting region in a state of equilibrium over a surface at a temperature of 302.7K (as discussed in section 3.b). As Table A1 shows, the effect of the correction term is to reduce the discrepancy in the equation from around 5% of the largest term to less than 1%. Similar impacts are observed in other configurations of the model, including in the coupled version.

The additional term expressed in the form in Eq. A12 will scale as approximately 20% of W_p in Eq. 3 , for a moist adiabiatic temperature profile where the lapse rate of the reference state Γ will be approximately half the dry adiabatic lapse rate $\frac{g}{c_p}$, where c_p is the specific heat capacity of dry air at constant pressure given that $\frac{R_v}{c_p}$=0.46.

References

Ambaum, M. H. P., 2010: *Thermal physics of the atmosphere*. John Wiley & Sons.

Daleu, C. L., S. Woolnough, and R. Plant, 2012: Cloud-resolving model simulations with one- and two-way couplings via the weak temperature gradient approximation. *Journal of the Atmospheric Sciences*, **69 (12)**, 3683–3699.

Daleu, C. L., S. J. Woolnough, and R. S. Plant, 2015a: Transition from suppressed to active convection modulated by a weak temperature gradient–derived large-scale circulation. *Journal of the Atmospheric Sciences*, **72 (2)**, 834–853.

Daleu, C. L., and Coauthors, 2015b: Intercomparison of methods of coupling between convection and large-scale circulation: 1. Comparison over uniform surface conditions. *Journal of Advances in Modeling Earth Systems*, **7**, 1576–1601.

Daleu, C. L., and Coauthors, 2016: Intercomparison of methods of coupling between convection and large-scale circulation: 2. Comparison over nonuniform surface conditions. *Journal of Advances in Modeling Earth Systems*, **8 (1)**, 387–405.

Emanuel, K., A. A. Wing, and E. M. Vincent, 2014: Radiative-convective instability. *Journal of Advances in Modeling Earth Systems*, **6 (1)**, 75–90.

Emanuel, K. A., 1986: An air-sea interaction theory for tropical cyclones. Part I: Steady-state maintenance. *Journal of the Atmospheric Sciences*, **43 (6)**, 585–605.

Gray, M., J. Petch, S. Derbyshire, A. Brown, A. Lock, H. Swann, and P. Brown, 2004: Version 2.3 of the Met Office Large Eddy Model: Part II. *Scientific documentation. Met Office, Exeter*.

Gray, M., J. Petch, S. Derbyshire, A. R. Brown, A. P. Lock, H. Swann, and P. Brown, 2001: Version 2.3 of the Met. Office Large Eddy Model. *Met Office (APR) Turbulence and Diffusion Rep*, **276**.

Herman, M. J., and D. J. Raymond, 2014: WTG cloud modeling with spectral decomposition. *Journal of Advances in Modeling Earth Systems*, **6**, 1121–1140.

Kuang, Z., 2008: Modeling the interaction between cumulus convection and linear gravity waves using a limited-domain cloud system–resolving model. *Journal of the Atmospheric Sciences*, **65 (2)**, 576–591.

Lorenz, E. N., 1960: Generation of available potential energy and the intensity of the general circulation. *Dynamics of Climate*, R. C. Pfeffer, Ed., Pergamon Press, Oxford, UK, 86–92.

Pauluis, O. M., 2011: Water vapor and mechanical work: A comparison of carnot and steam cycles. *Journal of the Atmospheric Sciences*, **68 (1)**, 91–102.

Pauluis, O. M., 2016: The mean air flow as Lagrangian dynamics approximation and its application to moist convection. *Journal of the Atmospheric Sciences*, **73 (4)**, 4407–4425.

Pauluis, O. M., V. Balaji, and I. M. Held, 2000: Frictional dissipation in a precipitating atmosphere. *Journal of the Atmospheric Sciences*, **57 (7)**, 989–994.

Pauluis, O. M., and I. M. Held, 2002a: Entropy budget of an atmosphere in radiative–convective equilibrium. Part I: Maximum work and frictional dissipation. *Journal of the Atmospheric Sciences*, **59 (2)**, 125–139.

Pauluis, O. M., and I. M. Held, 2002b: Entropy budget of an atmosphere in radiative–convective equilibrium. Part II: Latent heat transport and moist processes. *Journal of the Atmospheric Sciences*, **59 (2)**, 140–149.

Pauluis, O. M., and A. A. Mrowiec, 2013: Isentropic analysis of convective motions. *Journal of the Atmospheric Sciences*, **70 (11)**, 3673–3688.

Raymond, D. J., and X. Zeng, 2005: Modelling tropical atmospheric convection in the context of the weak temperature gradient approximation. *Quarterly Journal of the Royal Meteorological Society*, **131 (608)**, 1301–1320.

Romps, D. M., 2012: Weak pressure gradient approximation and its analytical solutions. *Journal of the Atmospheric Sciences*, **69 (9)**, 2835–2845.

Sobel, A. H., and C. S. Bretherton, 2000: Modeling tropical precipitation in a single column. *Journal of climate*, **13 (24)**, 4378–4392.

LIST OF TABLES

TABLE 1. Numerical values for the terms of Equation 3 for the control case of RCE in a single region. $\Delta\mathscr{G}$ is the unmodified Gibbs penalty component and Δ the corresponding discrepancy in the equation; $\Delta\mathscr{G}^*$ and Δ^* are the same quantities including the adjustment described in Appendix A.

(Wm^{-2})	W_{TdS}	W_b	W_p	$\Delta\mathscr{G}$	Δ	$\Delta\mathscr{G}^*$	Δ^*
Base case	11.17	2.18	3.14	6.32	-0.47	5.81	0.04
Pauluis (2016)	8.3	1.5	2.5	4.6	-0.3	-	-

LIST OF FIGURES

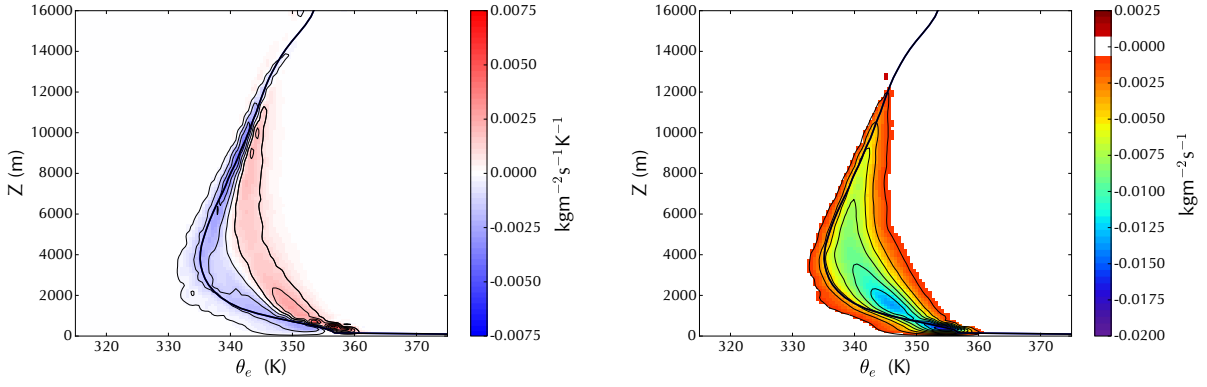

(a) Isentropic distribution of the vertical mass flux

(b) Isentropic stream function

FIG. 1. (a) Isentropic distribution and (b) streamfunction of the vertical mass flux $\langle \rho w \rangle$ for a single uncoupled region at RCE over an SST of 302.7 K. The solid line represents the mean profile of the equivalent potential temperature θ_e.

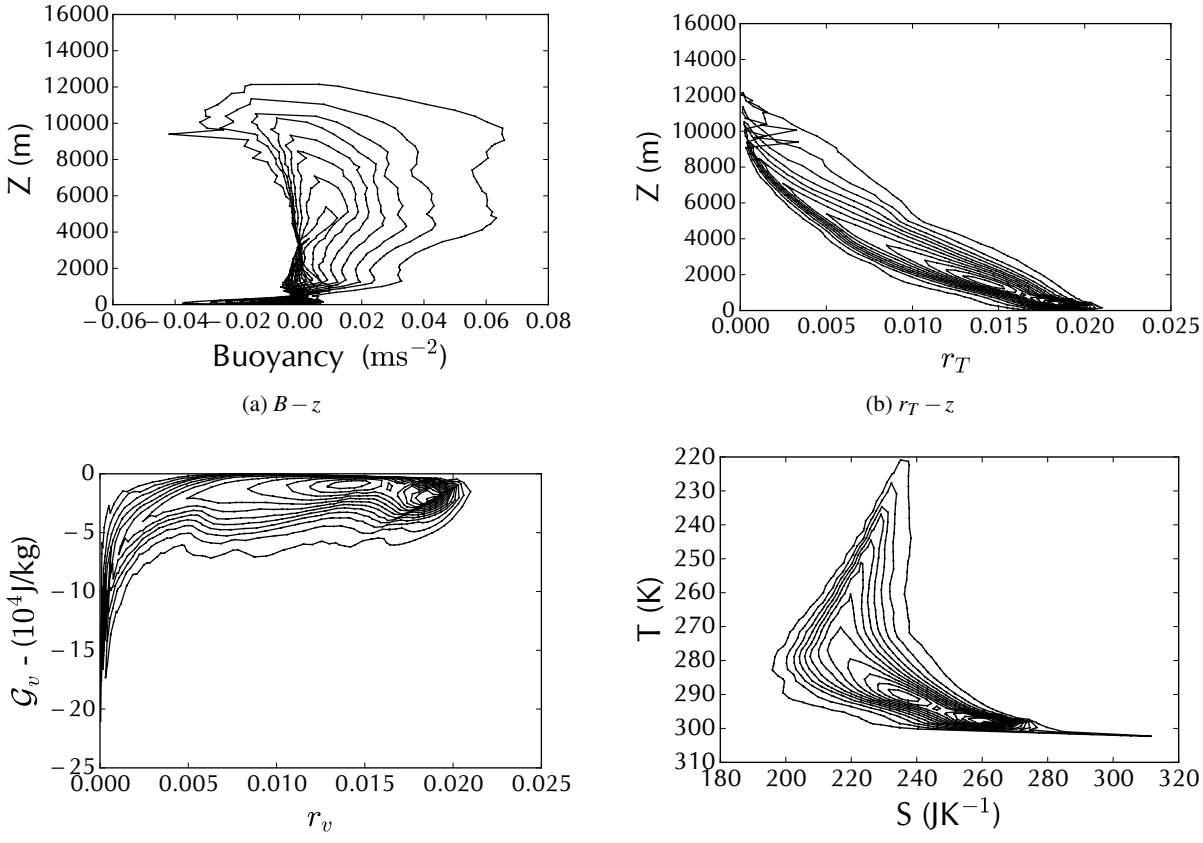

(a) $B-z$ (b) r_T-z

(c) $r_v-\mathscr{G}^*$ (d) $S-T$

644 FIG. 2. Thermodynamic diagrams for the main terms in Eq. 3 for a single uncoupled region at RCE over a
645 surface at temperature 302.7K showing 15 equally spaced contours of the streamfunction. (Numerical values
646 elsewhere in this paper were calculated using 60 contours.)

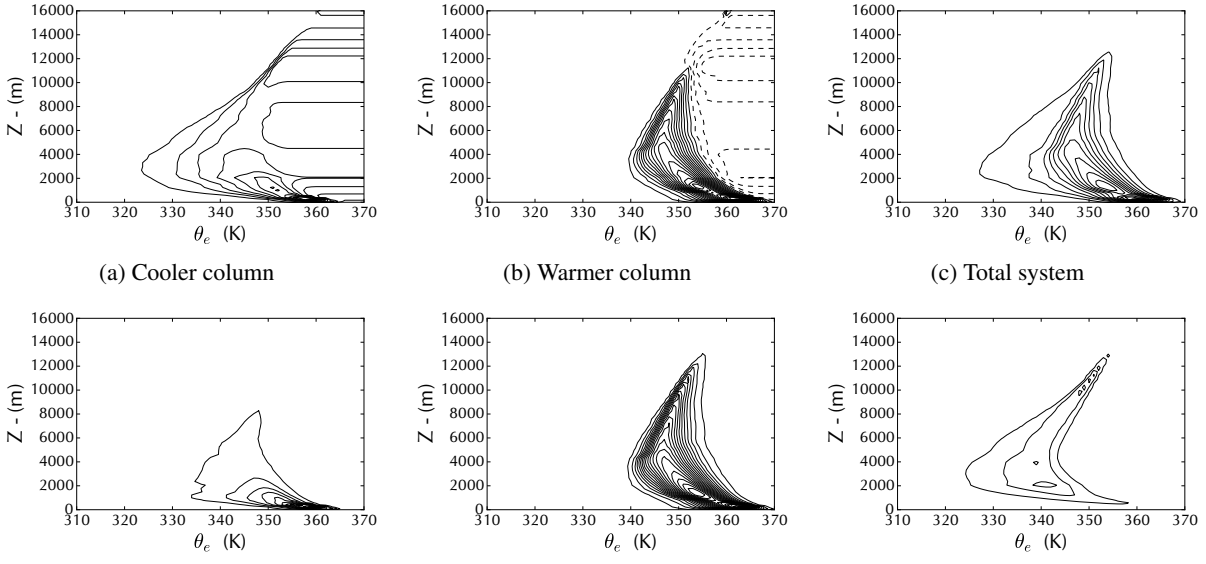

(a) Cooler column (b) Warmer column (c) Total system

(d) Cooler column - local (e) Warmer column - local (f) Large-scale circulation

FIG. 3. a) (b) Contours of the integrated vertical mass flux for each of the two regions analyed in isolation. The regions are run to RCE and are coupled with $\tau = 2$ hours. Note that the contours are not closed and so cannot be represented by a streamfunction. (c) shows the streamfunction of the total system. Once the large-scale circulation (f) is treated separately, the residual "convective" circulations in the two regions (d) and (e) exhibit closed contours. The same values for the contours are used in each of the plots; here solid lines indicate negative values and dashed lines positive values.

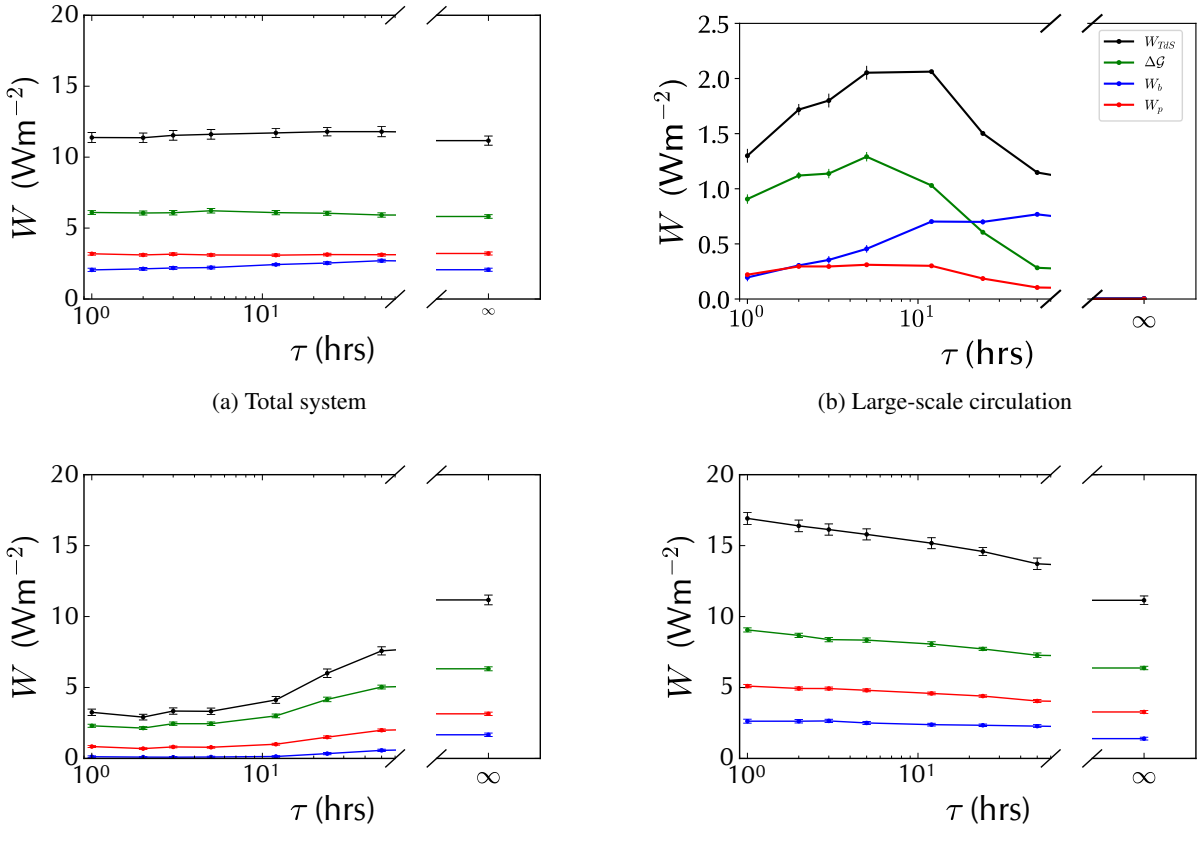

(a) Total system

(b) Large-scale circulation

(c) Cooler column

(d) Warmer column

653 FIG. 4. Components of Eq. 3 for (a) the total system, (b) the large-scale circulation and (c) (d) the convective
654 circulations in the cooler and warmer regions for varying coupling strengths. A high value of the coupling
655 timescale parameter τ indicates weak coupling. The blue line indicates W_b , the buoyancy work done, the red
656 W_p, the moisture elevator term, the green ΔG^*, the Gibbs penalty, and the black line W_{TdS} the Carnot maximum.
657 Error bars represent the standard error in the estimate of the parameter, obtained by subsampling.

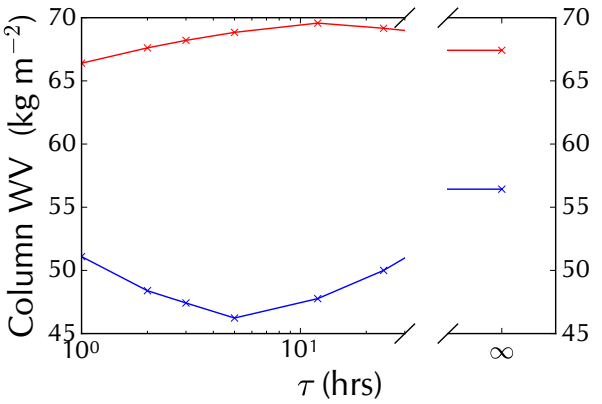

FIG. 5. Integrated column water vapour in the cool region (blue) and warm region (red) for varying values of WTG coupling relaxation timescale τ for an SST contrast of 2K.

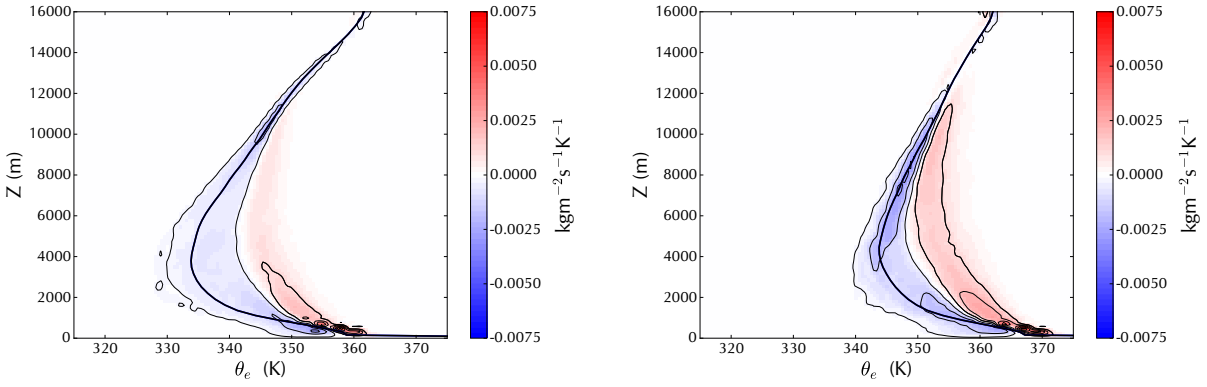

(a) Cooler column

(b) Warmer column

660 FIG. 6. Isentropic distribution of the vertical mass flux $\langle \rho w \rangle$ for (a) the cool region and (b) the warm region
661 with coupling τ = 50 hours. The solid line represents the mean profile of the equivalent potential temperature
662 θ_e.

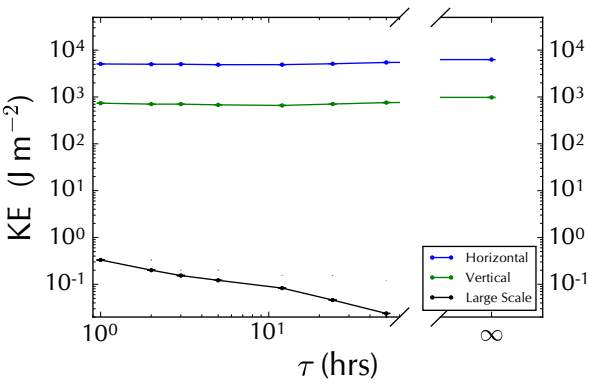

663 FIG. 7. Components of kinetic energy - the blue line represents the horizontal component and the green
664 line the vertical component for the aggregate system. The contribution of the large-scale motion to the vertical
665 kinetic energy is shown in black.

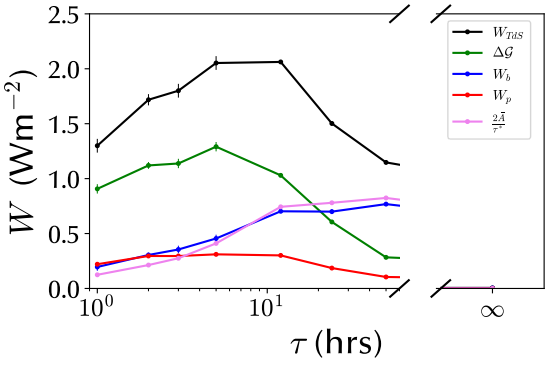

666 FIG. 8. As Fig. 4 (b). In addition the conversion rate from potential to kinetic energy based on Eq. 11 is
667 shown in violet.

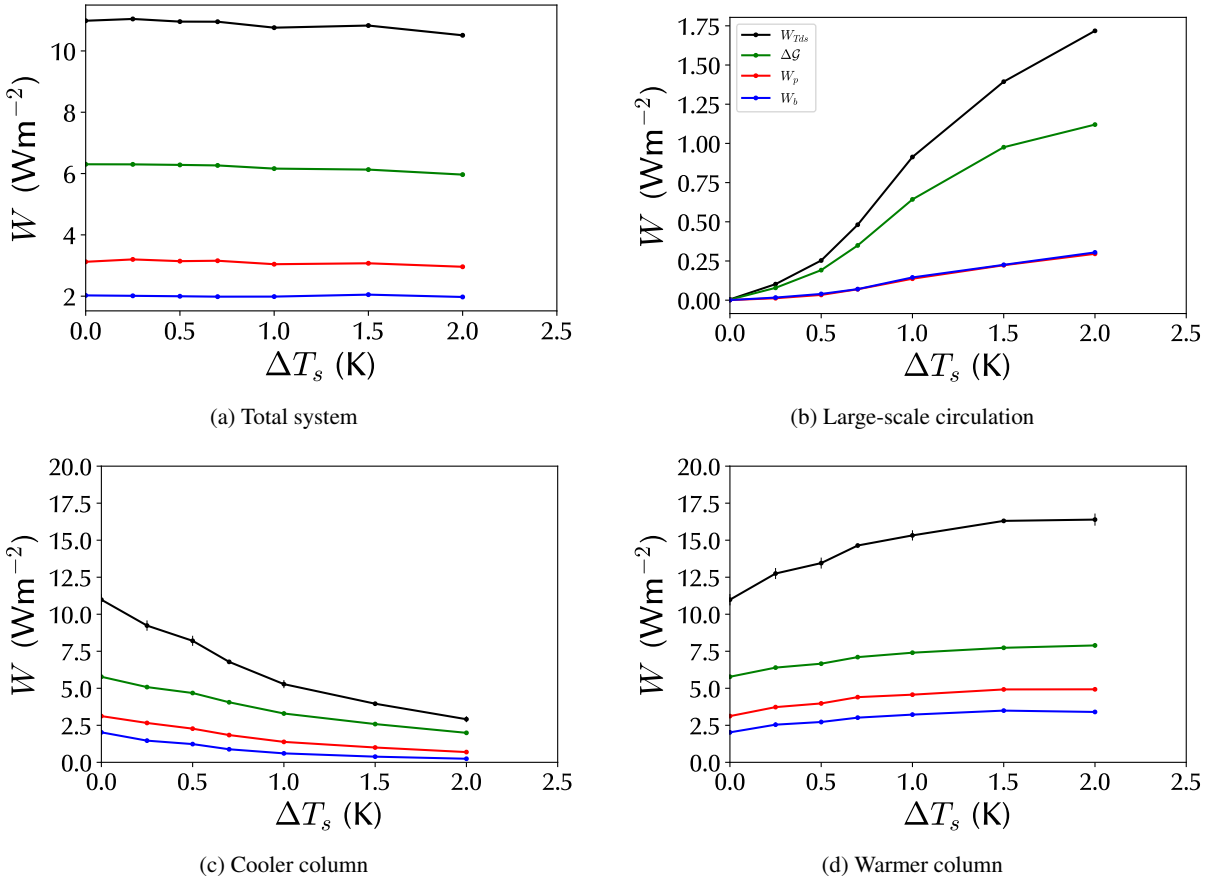

(a) Total system

(b) Large-scale circulation

(c) Cooler column

(d) Warmer column

668 FIG. 9. Components of Eq. 3 for (a) the total system, (b) the large-scale circulation and (c) (d) the convective
669 circulations in the cooler and warmer regions for varying values of ΔT_s, the difference between the SSTs in the
670 two regions. The blue line indicates W_b , the buoyancy work done, the red W_p, the moisture elevator term, the
671 green ΔG^*, the Gibbs penalty, and the black line W_{TdS} the Carnot maximum. In panel b) the red and blue lines
672 largely coincide

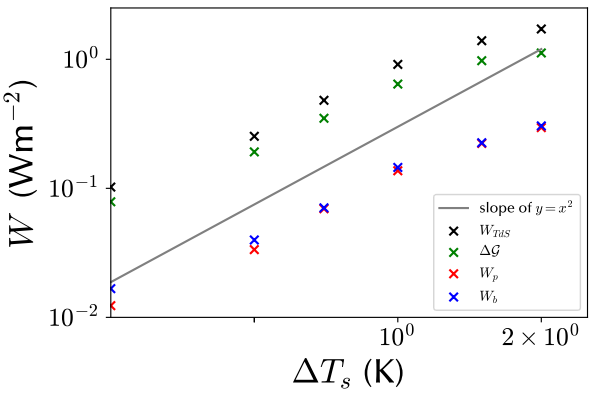

673 FIG. 10. Components of Eq. 3 for the large-scale circulation (as shown in Figure A9 ,but plotted on a log-log
674 scale) for varying values of ΔT_s, the difference between the SSTs in the two regions. The blue line indicates W_b ,
675 the buoyancy work done, the red W_p, the moisture elevator term, the green ΔG^*, the Gibbs penalty, and the black
676 line W_{TdS} the Carnot maximum.

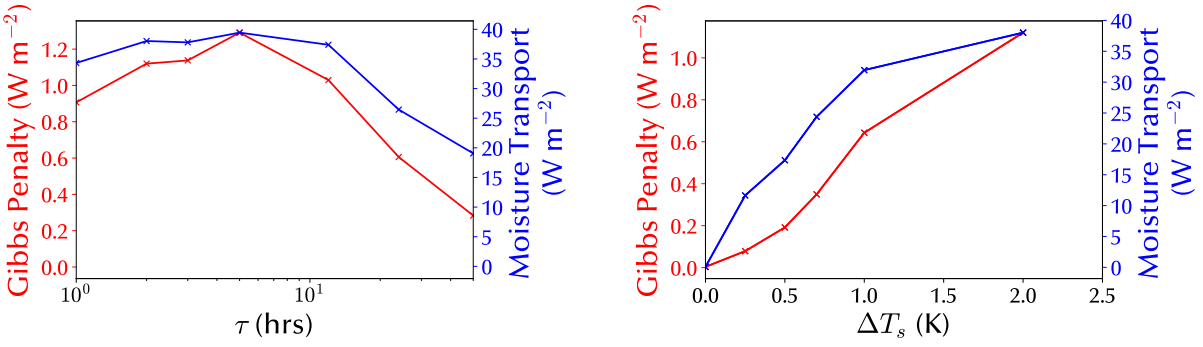

(a) Coupling strength

(b) SST difference

FIG. 11. Comparison between the Gibbs penalty component of the large-scale circulation (red, left hand axis) and latent heat transported between the regions (blue, right hand axis) for a) the numerical experiment where coupling strength is varied and b) the numerical experiment where SST difference is varied.